Inorganic Chemistry

ARTICLE

pubs.acs.org/IC

Experimental and Computational Investigation of Thiolate Alkylation in Ni^{II} and Zn^{II} Complexes: Role of the Metal on the Sulfur Nucleophilicity

Marcello Gennari,[†] Marius Retegan,[†] Serena DeBeer,[‡] Jacques Pécaut,[§] Frank Neese,[∥,⊥] Marie-Noëlle Collomb,[†] and Carole Duboc*[,†]

[†]Université Joseph Fourier Grenoble 1/CNRS, Département de Chimie Moléculaire, UMR-5250, Laboratoire de Chimie Inorganique Redox, Institut de Chimie Moléculaire de Grenoble FR, CNRS-2607, BP-53, 38041 Grenoble Cedex 9, France

[‡]Department of Chemistry and Chemical Biology, Cornell University, Ithaca, New York 14853, United States

[§]Laboratoire de Reconnaissance Ionique et Chimie de Coordination, Service de Chimie Inorganique et Biologique, UMR E-3 CEA/UJF, CNRS, CEA-Grenoble, INAC, 17 Rue des Martyrs 38054 Grenoble Cedex 9, France

[∥]Institute for Physical and Theoretical Chemistry, Universität Bonn, Wegelerstrasse 12, D-53113 Bonn, Germany

[⊥]Max-Planck-Institut für Bioanorganische Chemie, Stiftstrasse 34-36, D-45470 Mülheim an der Ruhr, Germany

Supporting Information

ABSTRACT: The biologically relevant S-alkylation reactions of thiolate ligands bound to a transition metal ion were investigated with particular attention paid to the role of the metal identity: Zn^{II} versus Ni^{II}. The reactivity of two mononuclear diamine dithiolate Zn and Ni complexes with CH_3I was studied. With the [ZnL] complex (**1**) (LH_2 = 2,2′-(2,2′-bipyridine-6,6′-diyl)bis(1,1-diphenylethanethiolate)), a double S-methylation occurs leading to $[ZnL^{Me2}I_2]$ ($\mathbf{1}^{Me2}$), while with [NiL] (**2**), only the mono-S-methylated product $[NiL^{Me}]I$ ($\mathbf{2}^{Me}$) is formed. Complexes **1** and $\mathbf{1}^{Me2}$ have been characterized by X-ray crystallography, while the structures of **2** and $\mathbf{2}^{Me}$ have been previously described. The kinetics of the first S-methylation reaction, investigated by ^1H NMR, is found to follow a second-order rate law, and the activation parameters, $\Delta H^{\ddagger}$ and $\Delta S^{\ddagger}$, are similar for both **1** and **2**. S K-edge X-ray absorption spectroscopy measurements have been carried out on **1**, **2**, and $\mathbf{2}^{Me}$, and a TD-DFT approach was employed to interpret the data. The electronic structures of **1** and **2** calculated by DFT reveal that the thiolate−metal bond is predominantly ionic in **1** and covalent in **2**. However, evaluation of the molecular electrostatic potential minima around the lone pairs of the thiolate sulfur atoms gives similar values for **1** and **2**, suggesting a comparable nucleophilicity. The DFT-optimized structures of the mono-S-methylation products have been calculated for the Zn and Ni complexes. Molecular electrostatic potential analysis of these products shows that (i) the nucleophilicity of the remaining thiolate sulfur atom is partly quenched for the Ni complex while it is conserved in the Zn complex and, more importantly, (ii) that the accessibility for the methyl transfer agent to the remaining thiolate is favored for the mono-S-methylated Zn complex compared to the Ni one. This explains the absence of a double S-methylation process in the case of the Ni complex at room temperature.

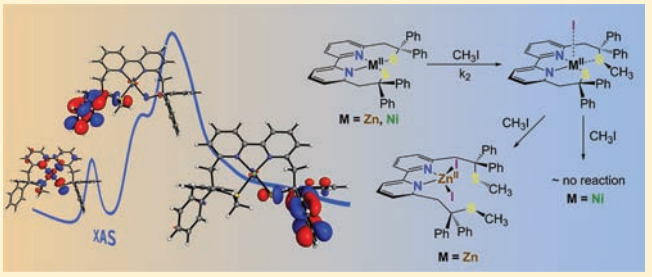

INTRODUCTION

Transition metal ions with thiolate ligands are found in the active sites of numerous metalloproteins and involved in a wide variety of biological processes.[1−4] Within this large family of metalloproteins, some active sites exploit the nucleophilicity of the thiolate sulfur atom to perform S-oxygenation and S-alkylation reactions.[5] Indeed, post-translational modifications in nitrile hydratase implicate S-oxygenation reactions via mononuclear thiolate Co^{III} or Fe^{III} active sites.[2] In addition, Zn^{II}-dependent thiolate methylation proteins have been identified including methionine synthase,[6] farnesyl transferase,[7] and, most prominently, the Ada protein implicated in DNA repair.[8]

In an effort to obtain insight into the S-alkylation mechanism of these Zn(II) metalloenzymes, the reactivity of synthetic mononuclear thiolate Zn^{II} complexes has been investigated in numerous studies.[9−21] Generally, S-alkylation reactions can follow two different pathways: (i) a dissociative mechanism, in which the metal−sulfur bond is split, followed by a S_N2 reaction involving the free thiolate and (ii) an associative mechanism, in which the reaction occurs via a S_N2 reaction involving the bound thiolate. It has been demonstrated that for anionic tetrathiolate Zn complexes a dissociative mechanism is operative,[10,22] while for neutral thiolate Zn complexes and for the Ada protein an associative mechanism is most likely.[11−13,23−26]

Received: April 28, 2011
Published: September 20, 2011

Scheme 1

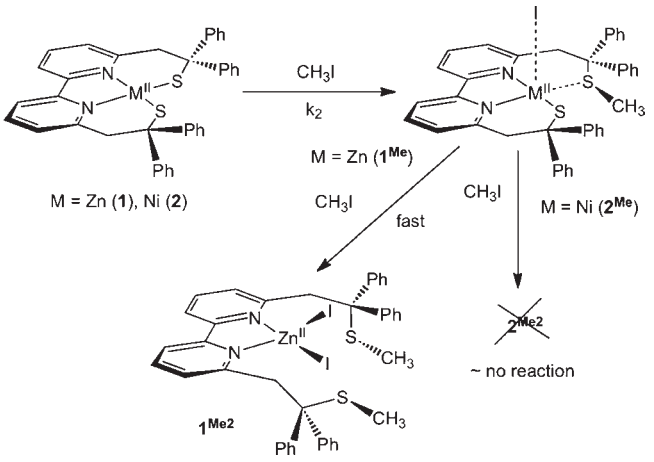

Even if none of the Ni thiolate-containing enzymes achieve S-oxygenation or S-alkylation reaction, synthetic mononuclear thiolate Ni complexes have also been extensively investigated because of their efficient reactions with dioxygen[5,27−31] or alkyl[15,32−37] transfer agent. It appears from these studies that series of mononuclear Ni^{II} and Zn^{II} thiolate complexes synthesized with the same ligand exhibit different reactivity toward S-alkylation. Indeed, the nature of the byproduct varies as a function of the metal: the resulting thioether remains generally bound to the Ni center, while it dissociates from the Zn center. For dithiolate complexes, only one sulfur atom is rapidly alkylated in the Ni complexes, while the mono-S-alkylated product is never isolated in the corresponding Zn complexes because of the very fast second S-alkylation reaction.

Thus, there is a need to define the factors that govern the nucleophilic reactivity of mononuclear Zn^{II} and Ni^{II} thiolate complexes with the aim of eventually being able to predict it. In this context, this work is focused on the reactivity toward CH_3I of two mononuclear dithiolate N_2S_2 Zn and Ni complexes, which has been rationalized by a deep investigation of their electronic structure. We report here the synthesis and characterization of the new mononuclear bisamine dithiolate N_2S_2 [ZnL] complex (**1**) (H_2L = 2,2′-(2,2′-bipyridine-6,6′-diyl)bis(1,1-diphenylethanethiol) (Scheme 1). We have shown that **1** reacts with CH_3I, generating the double S-methylated complex, $[ZnL^{Me2}I_2]$ ($\mathbf{1}^{Me2}$) (Scheme 1). We also compared the reactivity of **1** with that of the previously described isostructural Ni^{II} complex, [NiL] (**2**),[38] which leads to the mono-S-methylated complex, $[NiL^{Me}]I$ ($\mathbf{2}^{Me}$)[39] (Scheme 1). The S-methylation mechanism was investigated by kinetic experiments performed on **1** and **2**. S K-edge X-ray absorption spectroscopy (XAS) combined with quantum chemistry have been used to explore the electronic structures of the complexes **1**, **2**, and $\mathbf{2}^{Me}$ and especially the nature of the metal−thiolate bond, related to the reactivity of the initial and mono-S-methylated complexes.

RESULTS AND DISCUSSION

1. X-ray Structure of [ZnL] (1) and $[ZnL^{Me2}I_2]$ ($\mathbf{1}^{Me2}$). The structures of complexes **1** and $\mathbf{1}^{Me2}$ were determined by X-ray crystallography (Figure 1). Selected bond distances and angles are provided in Table 1. Complex **1** is crystallized in CH_2Cl_2 as a mononuclear dithiolate N_2S_2 Zn^{II} complex, as for the previously described Ni^{II} complex (**2**).[38] In contrast, in the presence of CuCl, the L^{2-} ligand reacts with CH_2Cl_2 to form a dinucleating ligand, leading to a dicopper complex.[40]

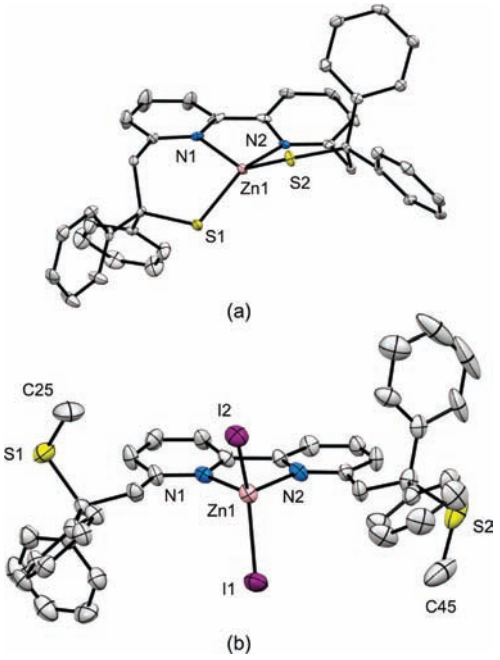

Figure 1. ORTEP drawing of (a) [ZnL] (**1**) and (b) $[ZnL^{Me2}I_2]$ ($\mathbf{1}^{Me2}$); 30% thermal ellipsoids. Hydrogen atoms are omitted for clarity.

Table 1. Selected Bond Lengths (Å) and Angles (deg) for [ZnL] (1) and $[ZnL^{Me2}I_2]$ ($\mathbf{1}^{Me2}$)

1		2	
Zn(1)−N(1)	2.116(5)	Zn(1)−N(1)	2.045(4)
Zn(1)−N(2)	2.117(5)	Zn(1)−N(2)	2.061(4)
Zn(1)−S(1)	2.271(2)	Zn(1)−I(1)	2.5432(7)
Zn(1)−S(2)	2.284(2)	Zn(1)−I(2)	2.5384(7)
		S(1)−C(25)	1.769(5)
		S(2)−C(45)	1.774(6)
N(1)−Zn(1)−N(2)	77.9(2)	N(1)−Zn(1)−N(2)	81.34(19)
N(1)−Zn(1)−S(1)	97.8(1)	N(1)−Zn(1)−I(1)	114.86(10)
N(1)−Zn(1)−S(2)	143.4(1)	N(1)−Zn(1)−I(2)	109.19(11)
N(2)−Zn(1)−S(1)	146.4(1)	N(2)−Zn(1)−I(1)	109.47(11)
N(2)−Zn(1)−S(2)	97.0(1)	N(2)−Zn(1)−I(2)	113.75(10)
S(1)−Zn(1)−S(2)	104.98(7)	I(1)−Zn(1)−I(2)	121.37(3)

The coordination sphere of the Zn^{II} ion consists of two nitrogen atoms of the bipyridine unit and two sulfur atoms of the aliphatic thiolates of L^{2-}. The geometry around the central Zn ion is in between a square plane and a tetrahedron, with a twist angle of 46.38° (angle between the NZnN and SZnS planes). In contrast, the corresponding Ni^{II} complex, **2**, displays a pseudo-square-planar geometry with a twist angle of 29.15°. The other previously described dithiolate N_2S_2 Zn^{II} complexes present geometries closer to a tetrahedron regardless of whether the ligands lead to 5- or 6-membered *N,S* chelates.[41−44] As expected, the Zn−S (2.271(2) and 2.284(2) Å) and Zn−N (2.116(5) and 2.117(5) Å) bond distances in **1** are slightly longer than those of

dx.doi.org/10.1021/ic200899w |*Inorg. Chem.* 2011, 50, 10047–10055

2 (Ni−S 2.173(1) and 2.176(1) Å; Ni−N 1.934(2) and 1.935(2) Å).

In the dimethyl complex $\mathbf{1}^{\mathbf{Me2}}$, the zinc anion is coordinated to two nitrogen atoms of the bipyridine units of L^{Me2} and two iodide ions in a pseudo-tetrahedral geometry with a twist angle of 85.95°. Coordination of the iodide ions to the Zn ion is confirmed by the typical Zn−I bond lengths observed in $\mathbf{1}^{\mathbf{Me2}}$ (2.5384(7) and 2.5384(7) Å).[11,45] On the other hand, the long Zn−S(CH_3) distances (5.87 and 5.89 Å) unambiguously establish that the thioethers are not bound to the metal, in contrast to $\mathbf{2}^{\mathbf{Me}}$. The Zn−N distances (2.045(4) and 2.061(4) Å) are significantly shorter than those of **1**. The I−Zn−I angle (121.37(3)°) is affected by the small N−Zn−N angle (81.34(19)°) that is dictated by the rigidity of the bipyridine unit.

2. Electrochemical Properties of [ZnL] (1). The electrochemical properties of **1** were investigated in DMF. The cyclic voltammogram displays a quasi reversible wave at $E_{1/2} = -1.95$ V vs Fc/Fc^+ (ΔE_p = 70 mV) corresponding to a one-electron reduction process (Figure S1, Supporting Information). On the positive potential side, an irreversible wave is observed at E_{p_a} = +0.43 V. These two redox processes are obviously ligand based, consistent with the filled d-orbital manifold of the Zn^{II} ion. The anodic wave is thus assigned to an oxidation occurring at the thiolate sites, while the cathodic wave is attributed to reduction of the bipyridine unit.

3. Methylation Studies. Reaction of **1** and **2** in the presence of an excess of CH_3I was studied in CH_2Cl_2, and the metal-containing products were analyzed by mass spectrometry. The S-methylation reaction is selective since in the case of the Zn complex only the doubly S-methylated complex $[ZnL^{Me2}I_2]$ ($\mathbf{1}^{\mathbf{Me2}}$) is formed, while in the case of the Ni complex, the mono-S-methylated complex $[NiL^{Me}]I$ ($\mathbf{2}^{\mathbf{Me}}$) is exclusively produced after 12 h (Figure S2, Supporting Information). Both products were characterized by X-ray crystallography (see above for $\mathbf{1}^{\mathbf{Me2}}$ and ref 39 for $\mathbf{2}^{\mathbf{Me}}$). The inability of the thioethers to coordinate to the Zn center in $\mathbf{1}^{\mathbf{Me2}}$ is consistent with previous studies demonstrating that upon S-alkylation the resulting thioether generally dissociates from the metal center.[9,12,23,43] Indeed, only a few examples of Zn products with bound thioether(s) have been characterized so far.[12,15] Conversely, upon S-alkylation, the generated thioether commonly remains bound to the Ni center.[34−37]

The S-alkylation reaction was monitored by ^{1}H NMR in $CDCl_3$ by the smooth decay of ^{1}H NMR resonances typical of the initial dithiolate metal complexes, with the concomitant appearance of features that are characteristic of the thioether metal products of the methylation. For determining the rates of the first S-methylation process, the decay of the ^{1}H NMR resonances of the initial species was monitored as a function of time (Figures S3 and S4, Supporting Information). Kinetic data were accumulated under pseudo-first-order conditions (large excess of CH_3I), and they can be fitted by assuming second-order behavior ($v = k_2[M^{II}L][CH_3I]$) for both systems (Scheme 1). The pseudo-first-order rate constants (k_{obs}) were determined as a function of the CH_3I concentration ($k_{obs} = k_2[CH_3I]$). The k_2 values (1.3×10^{-3} and 1.1×10^{-2} M^{-1} s^{-1} for **1** and **2**, respectively, at 21 °C) reveal that with Ni the rate of the first S-methylation is faster than with Zn (Table 2). The kinetic parameters of these reactions were determined by analyzing the temperature dependence of k_2 for both **1** and **2**. From the resulting Eyring plots displayed in Figure 2, the activation parameters $\Delta H^{\ddagger}$ and $\Delta S^{\ddagger}$ were extracted: for **1**, $\Delta H^{\ddagger}$ = 54(3) kJ·mol^{-1} and $\Delta S^{\ddagger} = -115(11)$ J·mol^{-1}·K^{-1}, and for **2**, $\Delta H^{\ddagger}$ = 47(4) kJ·mol^{-1} and $\Delta S^{\ddagger} = -123(12)$ J·mol^{-1}·K^{-1}. These values are comparable to those obtained on two isostructural monothiolate N_4S Ni and Zn complexes.[14] However, in the former study the Ni^{II} ion was high spin. Here, we confirm that the kinetics of the first S-methylation is comparable for Zn^{II} and low-spin Ni^{II} ions.

Table 2. Second-Order Rate Constants (k_2) for Reactions of 1 (1.1 mM) and 2 (1.4 mM) with CH_3I (mono-S-methylation) in $CDCl_3$ at Different Temperatures

	k_2 ($M^{-1}\cdot s^{-1}$)	
T (K)	**1**	**2**
285.4	$8.8(5) \times 10^{-4}$	$6.0(2) \times 10^{-3}$
294.0	$1.5(2) \times 10^{-3}$	$1.25(5) \times 10^{-2}$
302.5	$3.1(1) \times 10^{-3}$	$2.2(1) \times 10^{-2}$
311.1	$6.1(6) \times 10^{-3}$	$3.3(2) \times 10^{-2}$

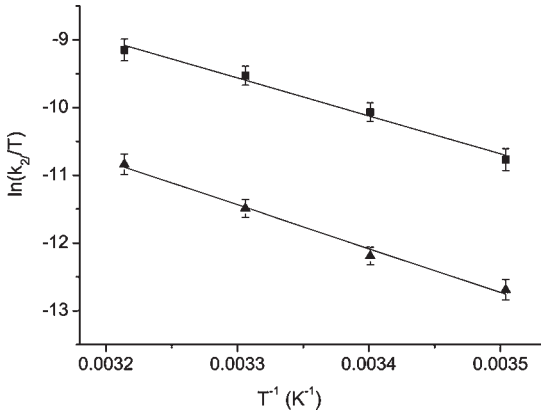

Figure 2. Eyring plots for reactions of **1** (▲) and **2** (■) with CH_3I in $CDCl_3$ determined by means of NMR data. Activation parameters derived from these plots are $\Delta H^{\ddagger}$ = +54(3) kJ·mol^{-1} and $\Delta S^{\ddagger} = -115(11)$ J·mol^{-1}·K^{-1} for **1** and $\Delta H^{\ddagger}$ = +47(4) kJ·mol^{-1} and $\Delta S^{\ddagger} = -123(12)$ J·mol^{-1}·K^{-1} for **2**.

The reaction exhibits an apparent second-order process for both Zn and Ni complexes, thus strongly suggesting that the same S_N2 mechanism is involved. Two mechanisms can be considered depending on the nature of the active nucleophilic species: the thiolate either is or is not coordinated to the metal center. On the basis of earlier studies, it is commonly assumed that for neutral complexes the mechanism is associative and does not involve a breaking of the thiolate−metal bond before the S-alkylation process.[13,14,24] The large negative activation entropies together with the small activation enthalpies values determined for **1** and **2** are also consistent with an associative mechanism.

All of our attempts to isolate the product of the mono-S-methylation of **1** have failed, revealing that the second S-alkylation is faster than the first one. In contrast, for the Ni complex, only the mono-S-methylated compound was isolated even in the presence of an excess of CH_3I after 12 h of reaction. Formation of traces of the bis-methylated $[NiL^{Me2}]^{2+}$ complex is only observed after 1 week of reaction at room temperature by mass spectrometry. This is consistent with the previous studies of Darensbourg, which showed that the second S-methylation of dithiolate Ni complexes is slower than the first one.[34]

Furthermore, in an attempt to understand the influence of the iodide on the reaction, we carried out S-methylation reactions

dx.doi.org/10.1021/ic200899w |Inorg. Chem. 2011, 50, 10047–10055

using a S-alkylating agent, which does not generate a coordinating counteranion, Me_3OBF_4. Mass spectrometry has shown that for the Ni complex only mono-S-methylation occurs like with CH_3I but the reaction is slower. For the Zn complex, we can only detect the L ligand even after 6 h of reaction using Me_3OBF_4. In contrast, with CH_3I, only the di-S-methylated ligand (L^{Me2}) is observed in the same conditions of reaction. These results indicate that the presence of the iodide is required to efficiently perform S-methylation reactions, especially for **1**.

In order to explain this difference in reactivity between the dithiolate Zn and Ni complexes for the S-methylation, we explored the electronic structure of the complexes by means of S K-edge XAS experiments and theoretical calculations.

4. Spectroscopic and Theoretical Investigation of the Methylation Process. *4.1. S K-Edge XAS Experiments.* The solid state S K-edge XAS of complexes **1**, **2**, and $\mathbf{2}^{Me}$ are shown in Figure 3. The principal results are reported in Table 3. The spectrum of **2** displays a pre-edge transition at 2470.5 eV, assigned to a transition from the S_{1s} orbital to the formally filled S_{3p} orbital, which gains hole character via mixing with a Ni 3d orbital (i.e., the transition corresponds to the lowest unoccupied molecular orbital with sulfur and metal character (LUMO)). The rising edge transition is located at 2472.4 eV. From the normalized intensity of the pre-edge, a semiquantitative measure of the Ni−S bond covalency can be estimated.[46−48] Plastocyanin was used as a reference, where it has been shown that 1.02 units of pre-edge intensity corresponds to 38% sulfur character in the singly occupied molecular orbital of the mononuclear Cu^{II} thiolate complex.[49] The pre-edge intensity of 1.16 normalized units thus corresponds to a contribution of 22% sulfur character in the LUMO of **2** (∼11% for each thiolate of L). For the previously described dithiolate [Ni(bme-daco)] (H_2-bme-daco = *N*,*N*′-bis-(2-mercaptoethyl)-1,5-diazacyclootane) complex, a larger contribution (23% for each thiolate) has been found.[50]

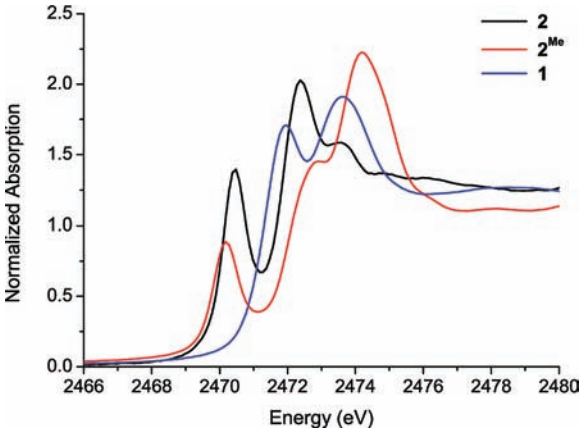

Figure 3. S K-edge XAS spectra of complexes **1**, **2**, and $\mathbf{2}^{Me}$.

Table 3. S K-Edge XAS Results

		exp. pre-edge energy (eV)	calcd pre-edge energy (eV)	exp. rising edge energy (eV)	calcd rising edge energy (eV)
2	RS^-	2470.5	2470.6	2472.4	2472.1
$\mathbf{2}^{Me}$	RS^-	2470.2	2470.3		2472.2
	$RSCH_3$		2472.4	2474.1	2473.6

The S K-edge XAS of $\mathbf{2}^{Me}$ displays three transitions at 2470.2, 2473.0, and 2474.1 eV. The pre-edge feature at 2470.2 eV is at similar energy and approximately 60% as intense as the pre-edge of **2** (0.65 arbitrary units). This mainly reflects the difference in the number of thiolate sulfur donors in both complexes (one and two in $\mathbf{2}^{Me}$ and **2**, respectively). From its intensity, the sulfur character of the LUMO can be experimentally estimated as ∼12%, a value comparable to that found for each thiolate in **2**.

The S K-edge XAS spectrum of the Zn^{II} complex (**1**) exhibits only two features at 2472.0 and 2473.6 eV. The absence of pre-edge feature in **1** is consistent with a d^{10} transition metal ion complex.

4.2. Theoretical Investigations. 4.2.1. S K-Edge XAS Analysis. The geometries of complexes **1**, **2**, and $\mathbf{2}^{Me}$ (denoted **1***, **2***, and $\mathbf{2}^{Me*}$) optimized with DFT (see computational details) were used as the basis for TD-DFT studies of the system's S K-edge spectra. The resulting optimized geometries compare well with the crystallographic data, thus validating the computational approach (Table 4).

By employing the TD-DFT approach, it has been shown that the pre-edge transition can be properly predicted in the case of thiolate−metal complexes.[51,52] Our calculations adequately reproduce the key features of the S K-edge XAS spectra of complexes **2** and $\mathbf{2}^{Me}$ (Figures S5 and S6, Supporting Information). For the two complexes, the energy of the pre-edge involving the thiolate ligand(s) located at around 2470 eV is well predicted (calculated 2470.6 and 2470.3 eV for **2*** and $\mathbf{2}^{Me*}$, respectively) (Table 3). For $\mathbf{2}^{Me*}$, the pre-edge transition involving the S-methylated thiolate ligand is calculated at 2472.4 eV, which is unfortunately overlapping with the rising edge of the thiolate ligand. This precludes determination of the normalized intensity of the pre-edge for the S-thioether in the experimental spectrum. Since the acceptor orbital is the same for both involved transitions, the relative energy of the S_{1s} orbital for a thiolate versus a thioether ligand can be measured from the difference of their pre-edge energies. The value of 2.1 eV is consistent with a previous study reporting that the S_{1s} orbital energy difference between a RS^- and a RSO_2^- ligand was 5.4 eV.[50] In fact, the

Table 4. Selected Bond Distances (Å) for the DFT Geometry-Optimized Models 1*, $\mathbf{1}^{Me(C)*}$, $\mathbf{1}^{Me(O)*}$, 2*, and $\mathbf{2}^{Me*}$ and Comparison (in parentheses) with the Experimental Data When Available

	M−S1	M−S2	M−N1	M−N2	M−I
1*	2.281 (2.271)	2.284 (2.284)	2.125 (2.116)	2.125 (2.117)	
$\mathbf{1}^{Me(C)*}$	2.312	2.817	2.143	2.201	2.610
$\mathbf{1}^{Me(O)*}$	2.267		2.069	2.158	2.573
2*	2.154 (2.173)	2.153 (2.176)	1.904 (1.934)	1.904 (1.935)	
$\mathbf{2}^{Me*}$	2.217 (2.169−2.174)	2.201 (2.172−2.187)	1.946 (1.899−1.914)	1.897 (1.918−1.959)	3.427 (3.778)

dx.doi.org/10.1021/ic200899w |*Inorg. Chem.* 2011, 50, 10047−10055

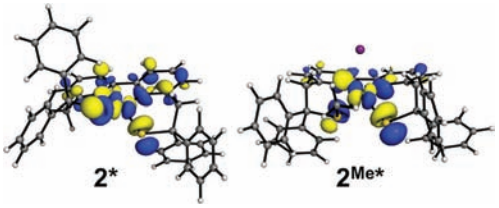

Figure 4. Contour plots of the LUMOs in **2*** and $\mathbf{2}^{\mathbf{Me}*}$.

S_{1s} orbital of an S-oxidized thiolate is much more stable than the corresponding orbital in an S-methylated thiolate.

The rising edge is more difficult to predict; however, our TD-DFT-calculated spectra are consistent with the experimental data (Figures S5 and S6, Supporting Information). Indeed, the predicted rising edge for **2** is properly reproduced (the experimental and calculated values are 2472.4 and 2472.1 eV, respectively). For $\mathbf{2}^{\mathbf{Me}*}$, the calculated energy of the rising edge implicating the thioether at 2473.6 eV is consistent with the experimental peak observed at 2474.1 eV (Figure 3).

The LUMO[53] has a total metal character of only 32% and 40% for **2*** and $\mathbf{2}^{\mathbf{Me}*}$, respectively, and also features strong σ-antibonding interactions with S_{3p} orbitals in both complexes (Figure 4). The S_{3p} character of the thiolate in the LUMO in **2*** is about 10% for each thiolate and 14% for the remaining thiolate in $\mathbf{2}^{\mathbf{Me}*}$, consistent with the S K-edge XAS experimental data (11% and 12% for **2** and $\mathbf{2}^{\mathbf{Me}}$, respectively). In $\mathbf{2}^{\mathbf{Me}*}$, the S_{3p} character of the thioether is smaller, about 6%. Note that these numbers do, of course, not represent physical observables. However, we found a very good agreement between theory and experiment.

The covalency of the Ni−$S_{thiolate}$ bond is greater than that of the Ni−$S_{thioether}$ bond given the S_{3p} character in the LUMO (14% and 6% for the thiolate and thioether in $\mathbf{2}^{\mathbf{Me}*}$, respectively). Furthermore, the combination of experimental and theoretical data demonstrates that the Ni−S covalency of the remaining thiolate in $\mathbf{2}^{\mathbf{Me}}$ is not affected by the presence of the neighboring thioether because of the comparable calculated value for the S_{3p} character of the thiolate in the LUMO (10% and 14% for **2*** and $\mathbf{2}^{\mathbf{Me}*}$, respectively). Equivalent strongly covalent Ni−$S_{thiolate}$ bonds therefore characterize both complexes.

4.2.2. Electronic Structures of the Dithiolate Zn and Ni Complexes. The Löwdin population analysis of complexes **1*** and **2*** is presented in Table 5. In the [ZnL] complex, the HOMO, nearly degenerate with the HOMO−1, is almost exclusively localized on the two thiolate sulfur atoms (36% for each), while for the [NiL] complex it also contains significant metal character (40% on Ni and 24% on each sulfur atom) (Figure 5). The π-antibonding nature of the HOMO found in **2*** and other Ni thiolate complexes has been previously used as the rationale for the increased nucleophilicity of the coordinated thiolates.[42] In **1***, the strong ionic character of the Zn−S bond compensates for the absence of the antibonding interactions, leading to a Zn complex which is just as nucleophilic as the Ni complex.[14] It is expected that these subtle electronic effects can be obtained from evaluation of the molecular electrostatic potential (MESP) around the lone pair region of the thiolate sulfur. Local minima of the MESP, denoted hereafter V_{min}, are usually observed in these regions where the electronic term dominates over the nuclear term. Determining MESP represents an interesting approach to assess the molecule's reactivity toward positively or negatively charged reactants, because it provides a good view of the relative polarity of a molecule. For both **1*** and **2***,

Table 5. Löwdin Population Analysis for the HOMO and Natural Population Analysis (NPA) Charges in Complexes 1*, $\mathbf{1}^{\mathbf{Me(C)}*}$, $\mathbf{1}^{\mathbf{Me(O)}*}$, 2*, and $\mathbf{2}^{\mathbf{Me}*}$

	molecular orbital composition (%)			NPA charges		
	M	S(1)[a]	S(2)[b]	M	S(1)[a]	S(2)[b]
1*	8	36	36	1.38	−0.48	−0.48
$\mathbf{1}^{\mathbf{Me(C)}*}$	7	68	<1	1.34	−0.52	0.21
$\mathbf{1}^{\mathbf{Me(O)}*}$	7	70	<1	1.34	−0.50	0.19
2*	40	24	24	0.65	−0.14	−0.14
$\mathbf{2}^{\mathbf{Me}*}$	43	18	1	0.69	−0.20	0.41

[a] S(1): thiolate sulfur atom. [b] S(2): thiolate or thioether sulfur atom.

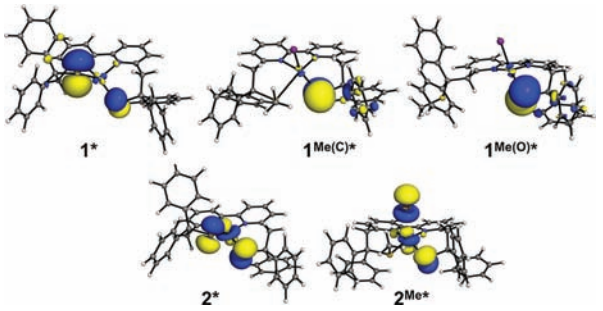

Figure 5. Contour plots of the HOMOs in **1***, $\mathbf{1}^{\mathbf{Me(C)}*}$, $\mathbf{1}^{\mathbf{Me(O)}*}$, **2***, and $\mathbf{2}^{\mathbf{Me}*}$.

we obtain similar values for the minima (−0.078 and −0.069 au for **1*** and **2***, respectively), suggesting that sulfur atoms in both complexes are characterized by a comparable nucleophilicity. This is in agreement with the available experimental data.

4.2.3. Electronic Structures of the Mono-S-Methylated Zn and Ni Complexes. Looking at the products observed in the presence of an excess of CH_3I, a second S-methylation reaction occurs exclusively with the Zn complex. To understand this result, the nucleophilicity of the remaining thiolate sulfur atom in the mono-S-methylated Zn^{II} and Ni^{II} complexes ($[ML^{Me}]I$ with M = Ni^{II} or Zn^{II}) was investigated.

While the product arising from the mono-S-methylation of the Ni complex, $\mathbf{2}^{\mathbf{Me}}$, has been isolated and characterized by X-ray crystallography, for the Zn complex, the rate of the second S-methylation in the Zn complex is too fast to isolate the mono-S-methylated Zn product. DFT calculations were thus used to predict the corresponding structure. Two optimized structures have been obtained. First, optimization has been initiated from the X-ray data of $\mathbf{2}^{\mathbf{Me}}$, in which the Ni^{II} ion has been substituted by Zn^{II}, and is denoted $\mathbf{1}^{\mathbf{Me(C)}*}$ (for the closed form). The second optimized structure is issued from the X-ray structure of $\mathbf{1}^{\mathbf{Me2}}$ and is denoted $\mathbf{1}^{\mathbf{Me(O)}*}$ (for the open form). The two structures have been conserved for the discussion since the difference in energy between these two structures is less than 1 kcal/mol and the energy barrier between them is also very small, meaning that both structures can be present in solution. The principal structural features of the DFT-optimized structure of $\mathbf{1}^{\mathbf{Me(C)}*}$, $\mathbf{1}^{\mathbf{Me(O)}*}$, and $\mathbf{2}^{\mathbf{Me}*}$ are given in Table 4. For $\mathbf{2}^{\mathbf{Me}*}$, the calculated structure compared well with the experimental data, unambiguously demonstrating that the thioether remains coordinated to the Ni^{II} center. Conversely for $\mathbf{1}^{\mathbf{Me(C)}*}$, the long Zn−$S_{Me}$ distance (2.817 Å) shows that this ligand is dissociated

dx.doi.org/10.1021/ic200899w |*Inorg. Chem.* 2011, 50, 10047–10055

Table 6. Wiberg Bond Indices Calculated for the Metal−Sulfur Bonds for Complexes 1^*, $1^{Me(C)}*$, $1^{Me(O)}*$, 2^*, and $2^{Me}*$

complexes	bond	Wiberg bond index
1^*	$Zn-S_{thiolate}$	0.35
$1^{Me(C)}*$	$Zn-S_{thiolate}$	0.32
	$Zn-S_{thioether}$	0.08
$1^{Me(O)}*$	$Zn-S_{thiolate}$	0.37
2^*	$Ni-S_{thiolate}$	0.55
$2^{Me}*$	$Ni-S_{thiolate}$	0.53
	$Ni-S_{thioether}$	0.41

from the metal ion. In fact, the $Zn-S_{thioether}$ bond lengths found in the rare examples of bound thioether Zn complexes are in the range 2.39−2.62 Å.[12,15] For $1^{Me(O)}*$, the Zn−N, Zn−I, and $Zn-S_{thiolate}$ bond distances are comparable to that of $1^{Me(C)}*$ while the $Zn-S_{thioether}$ bond length is notably increased leading to an open form.

The HOMOs for $1^{Me(C)}*$, $1^{Me(O)}*$, and $2^{Me}*$ are displayed in Figure 5. The HOMO of $2^{Me}*$ clearly reveals the loss of antibonding interactions at the $Ni-S_{Me}$ bond, and the contribution of the thioether sulfur atom to the HOMO becomes negligible (1%). However, the contribution of the thiolate sulfur atom to the HOMO in $2^{Me}*$ is still significant (18%) and cannot explain the lack of reactivity of the complex. Looking at $1^{Me(C)}*$ and $1^{Me(O)}*$, the thiolate sulfur atom mostly contributes to the HOMOs (68% and 70%, respectively), explaining that the second S-methylation occurs more rapidly than the first one.

The Wiberg bond indices calculated for all complexes (Table 6) reveal that the strength of the bonds varies in the order $Ni-S_{thiolate} \geq Ni-S_{thioether} \geq Zn-S_{thiolate} \gg Zn-S_{thioether}$. The small value calculated for the Wiberg bond index of the $Zn-S_{thioether}$ bond in $1^{Me(C)}*$ is consistent with dissociation of the sulfur atom from the Zn center. For the thiolate ligands, the interaction with the central Ni is slightly stronger than with Zn, as indicated by the increased Wiberg bond indices. On the other hand, the strengths of the $Ni-S_{thioether}$ and $Ni-S_{thiolate}$ bonds are similar, in agreement with comparable bond lengths (2.201 and 2.217 Å, respectively). Finally, no significant effect on the $M-S_{thiolate}$ bond in $1^{Me(C)}*$, $1^{Me(O)}*$, and $2^{Me}*$ is observed upon S-alkylation.

Natural population analysis (NPA) shows that the thiolate sulfur atom bears most of the negative charge in the complexes (−0.52, −0.50, and −0.20 for $1^{Me(C)}*$, $1^{Me(O)}*$, and $2^{Me}*$, respectively) (Table 5). We notice an increase of the negative charge compared to that of the initial complexes (−0.48 and −0.14 for 1^* and 2^*, respectively). At first glance, this result is in contradiction with the fact that no second S-methylation occurs with Ni. However, looking at the molecular electrostatic potential maps displayed in Figure 6, it clearly appears that the accessibility for the methyl transfer agent to the remaining thiolate is favored for $1^{MeO}*$ compared to $1^{Me(C)}*$ and $2^{Me}*$. The difference in steric hindrance is certainly an important factor to explain why a second S-methylation can occur in **1** and not in **2**. Furthermore, in the case of $2^{Me}*$, we find a magnitude for the minimum of the electrostatic potential of −0.052 au around the lone pair of the remaining thiolate sulfur atom, notably reduced with respect to that of 2^* (−0.069 au). In the case of the Zn complex, V_{min} is equal to −0.069 au for $1^{Me(C)}*$ and −0.075 au for $1^{Me(O)}*$, suggesting that the open form is the one that reacts with CH_3I. The V_{min} magnitude of $1^{Me(O)}*$ is higher than that of $2^{Me}*$ and similar to that of 1^* (−0.078 au). Consequently, these calculations indicate that the negative partial charge of the remaining thiolate sulfur is also partly quenched for the Ni complex compared to the Zn one.

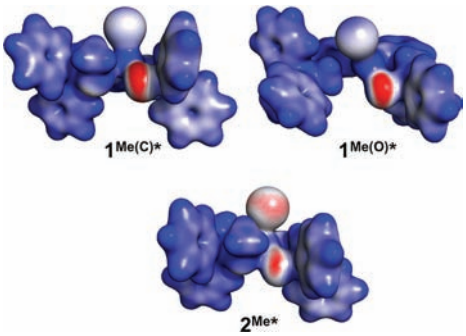

Figure 6. Electrostatic potential on the 0.02 au molecular surface for $1^{Me(C)}*$, $1^{Me(O)}*$, and $2^{Me}*$.

CONCLUDING REMARKS

The reactivity of mononuclear dithiolate N_2S_2 Ni and Zn complexes toward S-methylation was investigated by kinetic studies, and the results were tentatively rationalized by means of S K-edge XAS measurements combined with quantum chemistry. In the presence of an excess of CH_3I, a double S-methylation occurs in the case of the Zn complex, while for the Ni complex, only the mono-S-methylated product is formed at room temperature. However, the data show that a similar mechanism is operative for the first S-methylation in both Ni and Zn dithiolate complexes. This implicates that the nucleophilicity of the remaining thiolate sulfur atom is different in the mono-S-methylated Ni and Zn complexes. Besides, in the case of the Zn complex, the mono-S-methylated complex cannot be isolated given that the second reaction is faster than the first one.

The S K-edge XAS measurements show, as expected, that the $Ni-S_{thiolate}$ bond is highly covalent, while the character of the $Zn-S_{thiolate}$ bond appears to be ionic. However, evaluation of the minimum of the electrostatic potential of the thiolate sulfurs in both **1** and **2** complexes shows that their nucleophilicity is comparable, in agreement with the kinetic experiments. Regarding the second S-methylation process, which only occurs for the Zn complex, the difference in reactivity with the Ni complex can be rationalized by molecular electrostatic potential analysis. Indeed, this analysis suggests (i) that the nucleophilicity of the remaining thiolate in the Ni complex is partly quenched while it is conserved in the case of the Zn complex and, more importantly, (ii) that the accessibility for the methyl transfer agent to the remaining thiolate is favored for the mono-S-methylated Zn complex compared to the Ni one.

This work represents a nice example to show how powerful the combination of experimental and theoretical investigation is to understand the relation between the reactivity and the electronic structure of transition metal ion complexes.

EXPERIMENTAL SECTION

General. The ligand H_2L[54] and complexes [NiL] (**2**)[38] and [NiL^{Me}]I (2^{Me})[39] were prepared according to reported methods. THF and CH_2Cl_2 were freshly distilled (over Na/benzophenone and CaH_2, respectively)

prior to use. All other reagents and solvents were used as received. Synthesis of [ZnL] (**1**) was performed under argon (Schlenk techniques).

Synthesis of [ZnL] (1). Solid NaH (60% in mineral oil, 12.8 mg, 0.320 mmol) was added to a solution of H_2L (100 mg, 0.128 mmol) in THF (15 mL). After 20 min, the excess of NaH was filtered off and a solution of $Zn(OCOCH_3)_2$ (24 mg, 0.131 mmol) in MeOH:THF 1:4 (5 mL) was added, yielding a clear yellow precipitate. After 1 h, the solvents were removed in vacuo and the product was extracted from the residue with CH_2Cl_2 (35 mL). CH_2Cl_2 was then removed in vacuo, and the residual solid was washed with CH_3OH (3 × 5 mL) and recrystallized from CH_2Cl_2:CH_3OH 2:1, yielding a clear yellow microcrystalline solid (65 mg, 0.101 mmol, 79% yield). IR (cm^{-1}): 3055w, 3024w, 2923w, 1598s, 1574m, 1487m, 1441m, 1268w, 1175w, 1078w, 1035w, 1022w, 804w, 793w, 754w, 742m, 695s, 592 m. ^1H NMR (500 MHz, $CDCl_3$): δ 3.97 (s, 4H, CH_2), 6.60 (d, J = 7.7 Hz, 2H, CH bpy), 7.10 (m, 12H, CH Ph), 7.36 (d, J = 7.6 Hz, 8H, CH Ph), 7.60 (t, J = 7.8 Hz, 2H, CH bpy), 7.90 (d, J = 7.8 Hz, 2H, CH bpy). ESI-MS (10^{-5} M, CH_2Cl_2:CH_3CN, m/z, I%): 643.1, 100 $[ZnLH]^+$. Anal. Calcd for $C_{38}H_{30}N_2S_2Zn$ (644.17): C, 70.85; H, 4.69; N, 4.35. Found: C, 70.93; H, 4.61; N, 4.28. Colorless X-ray suitable single crystals of **1** were obtained by layering CH_3OH over a saturated solution of the product in CH_2Cl_2.

Obtaining of Single X-ray Crystals of $[ZnL^{Me2}I_2]$ (1^{Me2}). Colorless single crystals of $[ZnL^{Me2}I_2]$ (1^{Me2}) were obtained by slow evaporation of a CH_2Cl_2:CH_3OH (1:1) solution of [ZnL], which was previously treated with CH_3I (20 equiv) in CH_2Cl_2 for 12 h. ^1H NMR (500 MHz, $CDCl_3$): δ 1.87 (s, 6H, CH_3), 4.93 (s, 4H, CH_2), 7.21 (t, J = 7.3 Hz, 4H, CH Ph), 7.34 (t, J = 7.7 Hz, 8H, CH Ph), 7.61 (d, J = 8.0 Hz, 2H, CH bpy), 7.66 (d, J = 7.8 Hz, 8H, CH Ph), 7.76 (t, J = 8.0 Hz, 2H, CH bpy), 7.90 (d, J = 7.9 Hz, 2H, CH bpy).

Physical Measurements. The infrared spectrum of **1** was recorded on a Magna-IR TM 550 Nicolet spectrometer as a KBr pellet. ^1H NMR spectra were recorded on a Varian Unity+ 500 MHz spectrometer. Elemental analysis of **1** was carried out with a C, H, N analyzer (SCA, CNRS).

Kinetic Measurements. For reactions of **1** and **2** with CH_3I, the rates of the first S-methylation process were measured by ^1H NMR spectroscopy in pseudo-first-order conditions (i.e., in the presence of a fixed concentration of complex and a large excess of CH_3I) by monitoring the decay of the resonances of the initial complexes (in both cases the CH_2 singlet of the coordinated ligand L^{2-}) as a function of time. Standard solutions of the complexes (1.3 mM of **1**, 1.6 mM of **2**) and CH_3I (0.80 and 6.96 M) were prepared in $CDCl_3$ and stored at 4 °C in the dark. The reagents (and further $CDCl_3$) were combined in a NMR sample tube immediately prior to measurements (final concentrations 1.1 mM of **1** + 33−522 mM range of CH_3I, 1.4 mM of **2** + 5−80 mM range of CH_3I). After being mixed thoroughly, the tube was placed in a thermostat probe of an NMR spectrometer. ^1H NMR spectra were recorded throughout the reaction. The integrated intensities I of the CH_2 singlet at 3.9 and 4.1 ppm for **1** and **2**, respectively, provide a relative measurement of the concentration of the initial complex in each spectrum. Pseudo-first-order rate constants (k_{obs}) were determined from the slopes of first-order plots, $-\ln I$ versus time (Tables S2−S9, Supporting Information), at different analytical concentrations of CH_3I and temperatures (285.4, 294.0, 302.5, 311.1 K). Second-order rate constants k_2 were determined using the relationship $k_{obs} = k_2[CH_3I]$ for each temperature (Table 2). An Eyring analysis of the temperature dependence of k_2 yielded activation parameters $\Delta H^{\ddagger}$ and $\Delta S^{\ddagger}$ (Figure 2).

ESI-MS Experiments. ESI-MS experiments were performed on a Bruker Esquire 3000 Plus ion trap spectrometer equipped with an electrospray ion source (ESI). Samples were prepared at 30 °C by mixing 5 mL of a solution of **1** or **2** (0.6 mM of in CH_2Cl_2) with 20 equiv (200 μL) of a solution of MeI or Me_3OBF_4 (0.63 M in MeOH:CH_2Cl_2 1:9). The solutions have been analyzed after 3 min and 6 and 15 h (only in the case of MeI for 15 h) of reaction in positive ionization mode by direct perfusion in the ESI-MS interface after dilution to 5×10^{-5} M with MeCN. All instrumental parameters remained unchanged for all measurements (ESI capillary voltage 2 kV, sampling cone voltage 40 V).

ESI-MS (m/z, I%) of **1** + MeI: after 3 min 643.1, 100 $[ZnLH]^+$, 579.5, 90 $[LH]^+$; after 6 and 15 h 609.1, 100 $[L^{Me2}H]^+$, 671.1, 5 $[ZnL^{Me2}H]^+$ (see Figure S2, Supporting Information). ESI-MS (m/z, I%) of **2** + MeI: after 3 min and 6 and 15 h: 651.1, 100 $[NiL^{Me}]^+$ (see Figure S2, Supporting Information). ESI-MS (m/z, I%) of **1** + Me_3OBF_4: after 3 min and 6 h 581.1, 100 $[LH_3]^+$. ESI-MS (m/z, I%) of **2**+Me_3OBF_4: after 3 min 637.2, 100 $[NiLH]^+$; after 6 h 637.2, 100 $[NiLH]^+$, 651.4, 20 $[NiL^{Me}]^+$.

S K-Edge XAS. All data were measured at the Stanford Synchrotron Radiation Lightsource under ring conditions of 3.0 GeV and 60−100 mA. S K-edge data were measured using beamline 4-3. A fully tuned Si(111) monochromator was utilized for energy selection, and a Ni-coated mirror was utilized for rejection of higher harmonics. All samples were measured at room temperature as fluorescence spectra using a Lytle detector. Samples were ground finely and dispersed as thinly as possible on Mylar tape to minimize the possibility of fluorescence saturation effects. Data represent 2−3 scan averages. All samples were monitored for photoreduction throughout the course of data collection. The S K-edge energy was calibrated using the S K-edge spectra of $Na_2S_2O_3 \cdot 5H_2O$, run at intervals between sample scans. The maximum of the first pre-edge feature in the spectrum was fixed at 2472.02 eV. A step size of 0.08 eV was used over the edge region. Data were averaged, and a smooth background was removed from all spectra by fitting a polynomial to the pre-edge region and subtracting this polynomial from the entire spectrum. Normalization of the data was accomplished by fitting a flattened polynomial or straight line to the postedge region and normalizing the postedge to 1.0.

X-ray Crystallography. A summary of data collection and structure refinement for **1** and $\mathbf{1}^{Me2}$ is reported in Table S1, Supporting Information. Single-crystal diffraction data of **1** were taken using a Bruker AXS Enraf-Nonius Kappa CCD diffractometer. The molecular structure was solved by direct methods and refined with the TEXSAN software package. Single-crystal diffraction data of $\mathbf{1}^{Me2}$ were taken using an Oxford-Diffraction Xcallibur S Kappa geometry diffractometer (Mo Kα radiation, graphite monochromator, λ 0.71073 Å) at 150 K. An absorption correction was applied using the ABSPACK Oxford-diffraction program[55] with transmission factors in the range from 0.623 to 0.940. The molecular structure of $\mathbf{1}^{Me2}$ was solved by direct methods and refined on F^2 by full matrix least-squares techniques using the SHELXTL package.[56] All non-hydrogen atoms were refined anisotropically, and hydrogen atoms were placed at their calculated position.

Electrochemistry. Electrochemical measurements were carried out under an argon atmosphere (in glovebox at room temperature). Cyclic voltammetry experiments were performed by using an EG&G model 173 potentiostat/galvanostat equipped with a PAR model universal programmer. A standard three-electrode electrochemical cell was used. Potentials were referred to an Ag/0.01 M $AgNO_3$ reference electrode in CH_3CN + 0.1 M Bu_4NClO_4. Measured potentials were calibrated through the use of an internal Fc/Fc^+ standard. The working electrode was a vitreous carbon disk (3 mm in diameter) polished with 2 μm diamond paste (Mecaprex Presi) for cyclic voltammetry (E_{p_a}, anodic peak potential; E_{p_c}, cathodic peak potential; $E_{1/2} = (E_{p_a} + E_{p_c})/2$; $\Delta E_p = E_{p_a} - E_{p_c}$). The auxiliary electrode was a Pt wire in DMF + 0.1 M Bu_4NPF_6 solution.

Computational Details. All calculations were performed with the ORCA quantum chemistry program package.[57] Geometry optimizations were carried out using the BP86 functional,[58,59] the zeroth-order regular approximation for relativistic effects (ZORA),[60,61] and the scalar relativistic recontraction of the def2-TZVP basis sets.[62] In all calculations we took advantage of the RI approximation using the Coulomb-fitting basis

set of Weigend.[63] A dense integration grid was used (ORCA grid4), coupled with tight SCF convergence criteria.

XAS spectra were calculated by employing time-dependent density functional theory (TD-DFT) on the optimized geometries, as detailed previously.[51] These calculations were done analogously to the geometry optimizations, with the sole exception of uncontracting the density-fitting basis set.

The local minimum of the molecular electrostatic potential (MESP) around the lone pair region of the sulfur thiolate atom was determined by employing a grid search technique on a cubic grid (width 101 points/side).

■ ASSOCIATED CONTENT

Supporting Information. Cif files of **1** and $\mathbf{1}^{Me2}$; additional structural, electrochemical, and S K-edge XAS data; complementary data on kinetic investigations; further computational details. This material is available free of charge via the Internet at http://pubs.acs.org.

■ AUTHOR INFORMATION

Corresponding Author
*E-mail: carole.duboc@ujf-grenoble.fr.

■ ACKNOWLEDGMENT

M.G. thanks the CNRS for his postdoctoral fellowship. The authors thank B. Gerey for his participation to some experiments. S.D. acknowledges Cornell University for financial support. Portions of the data in this paper were obtained at SSRL. SSRL operations are funded by the Department of Energy, Office of Basic Energy Sciences. The Structural Molecular Biology program is supported by the National Institutes of Health (grant 5 P41 RR001209), National Center for Research Resources, Biomedical Technology Program, and Department of Energy, Office of Biological Environmental Research.

■ REFERENCES

(1) Solomon, E. I.; Gorelsky, S. I.; Dey, A. *J. Comput. Chem.* **2006**, *27*, 1415.
(2) Kovacs, J. A. *Chem. Rev.* **2004**, *104*, 825.
(3) Venkateswara Rao, P.; Holm, R. H. *Chem. Rev.* **2003**, *104*, 527.
(4) Wuerges, J.; Lee, J.-W.; Yim, Y.-I.; Yim, H.-S.; Kang, S.-O.; Djinovic Carugo, K. *Proc. Natl. Acad. Sci. U.S.A.* **2004**, *101*, 8569.
(5) Grapperhaus, C. A.; Darensbourg, M. Y. *Acc. Chem. Res.* **1998**, *31*, 451.
(6) Peariso, K.; Zhou, Z. H. S.; Smith, A. E.; Matthews, R. G.; Penner-Hahn, J. E. *Biochemistry* **2001**, *40*, 987.
(7) Tobin, D. A.; Pickett, J. S.; Hartman, H. L.; Fierke, C. A.; Penner-Hahn, J. E. *J. Am. Chem. Soc.* **2003**, *125*, 9962.
(8) Myers, L. C.; Terranova, M. P.; Ferentz, A. E.; Wagner, G.; Verdine, G. L. *Science* **1993**, *261*, 1164.
(9) Wilker, J. J.; Lippard, S. J. *J. Am. Chem. Soc.* **1995**, *117*, 8682.
(10) Wilker, J. J.; Lippard, S. J. *Inorg. Chem.* **1997**, *36*, 969.
(11) Grapperhaus, C. A.; Tuntulani, T.; Reibenspies, J. H.; Darensbourg, M. Y. *Inorg. Chem.* **1998**, *37*, 4052.
(12) Hammes, B. S.; Carrano, C. J. *Inorg. Chem.* **2001**, *40*, 919.
(13) Warthen, C. R.; Hammes, B. S.; Carrano, C. J.; Crans, D. C. *J. Biol. Inorg. Chem.* **2001**, *6*, 82.
(14) Fox, D. C.; Fiedler, A. T.; Halfen, H. L.; Brunold, T. C.; Halfen, J. A. *J. Am. Chem. Soc.* **2004**, *126*, 7627.
(15) Grapperhaus, C. A.; Mullins, C. S.; Mashuta, M. S. *Inorg. Chim. Acta* **2005**, *358*, 623.
(16) Morlok, M. M.; Janak, K. E.; Zhu, G.; Quarless, D. A.; Parkin, G. *J. Am. Chem. Soc.* **2005**, *127*, 14039.
(17) Ji, M.; Benkmil, B.; Vahrenkamp, H. *Inorg. Chem.* **2005**, *44*, 3518.
(18) Ibrahim, M. M.; He, G.; Seebacher, J.; Benkmil, B.; Vahrenkamp, H. *Eur. J. Inorg. Chem.* **2005**, *2005*, 4070.
(19) Rombach, M.; Seebacher, J.; Ji, M.; Zhang, G. F.; He, G. S.; Ibrahim, M. M.; Benkmil, B.; Vahrenkamp, H. *Inorg. Chem.* **2006**, *45*, 4571.
(20) Melnick, J. G.; Zhu, G.; Buccella, D.; Parkin, G. *J. Inorg. Biochem.* **2006**, *100*, 1147.
(21) Notni, J.; Günther, W.; Anders, E. *Eur. J. Inorg. Chem.* **2007**, *2007*, 985.
(22) Wilker, J. J.; Wetterhahn, K. E.; Lippard, S. J. *Inorg. Chem.* **1997**, *36*, 2079.
(23) Brand, U.; Rombach, M.; Seebacher, J.; Vahrenkamp, H. *Inorg. Chem.* **2001**, *40*, 6151.
(24) Chiou, S. J.; Riordan, C. G.; Rheingold, A. L. *Proc. Natl. Acad. Sci. U.S.A.* **2003**, *100*, 3695.
(25) Bridgewater, B. M.; Fillebeen, T.; Friesner, R. A.; Parkin, G. *J. Chem. Soc., Dalton Trans.* **2000**, 4494.
(26) Chiou, S.-J.; Innocent, J.; Riordan, C. G.; Lam, K.-C.; Liable-Sands, L.; Rheingold, A. L. *Inorg. Chem.* **2000**, *39*, 4347.
(27) Kaasjager, V. E.; Bouwman, E.; Gorter, S.; Reedijk, J.; Grapperhaus, C. A.; Reibenspies, J. H.; Smee, J. J.; Darensbourg, M. Y.; Derecskei-Kovacs, A.; Thomson, L. M. *Inorg. Chem.* **2002**, *41*, 1837.
(28) Maroney, M. J.; Choudhury, S. B.; Bryngelson, P. A.; Mirza, S. A.; Sherrod, M. J. *Inorg. Chem.* **1996**, *35*, 1073.
(29) Henderson, R. K.; Bouwman, E.; Spek, A. L.; Reedijk, J. *Inorg. Chem.* **1997**, *36*, 4616.
(30) Mullins, C. S.; Grapperhaus, C. A.; Frye, B. C.; Wood, L. H.; Hay, A. J.; Buchanan, R. M.; Mashuta, M. S. *Inorg. Chem.* **2009**, *48*, 9974.
(31) Chohan, B. S.; Maroney, M. J. *Inorg. Chem.* **2006**, *45*, 1906.
(32) Farmer, P. J.; Reibenspies, J. H.; Lindahl, P. A.; Darensbourg, M. Y. *J. Am. Chem. Soc.* **1993**, *115*, 4665.
(33) Musie, G.; Reibenspies, J. H.; Darensbourg, M. Y. *Inorg. Chem.* **1998**, *37*, 302.
(34) Bellefeuille, J. A.; Grapperhaus, C. A.; Derecskei-Kovacs, A.; Reibenspies, J. H.; Darensbourg, M. Y. *Inorg. Chim. Acta* **2000**, *300*−*302*, 73.
(35) Green, K. N.; Brothers, S. M.; Jenkins, R. M.; Carson, C. E.; Grapperhaus, C. A.; Darensbourg, M. Y. *Inorg. Chem.* **2007**, *46*, 7536.
(36) Smee, J. J.; Miller, M. L.; Grapperhaus, C. A.; Reibenspies, J. H.; Darensbourg, M. Y. *Inorg. Chem.* **2001**, *40*, 3601.
(37) Grapperhaus, C. A.; Kreso, M.; Burkhardt, G. A.; Roddy, J. V. F.; Mashuta, M. S. *Inorg. Chim. Acta* **2005**, *358*, 123.
(38) Gennari, M.; Orio, M.; Pécaut, J.; Neese, F.; Collomb, M.-N.; Duboc, C. *Inorg. Chem.* **2010**, *49*, 6399.
(39) Gennari, M.; Orio, M.; Pécaut, J.; Bothe, E.; Neese, F.; Collomb, M.-N.; Duboc, C. *Inorg. Chem.* **2011**, *50*, 3707.
(40) Gennari, M.; Pécaut, J.; DeBeer, S.; Neese, F.; Collomb, M.-N.; Duboc, C. *Angew. Chem., Int. Ed.* **2011**, *50*, 5662.
(41) Alves de Sousa, R.; Galardon, E.; Rat, M.; Giorgi, M.; Artaud, I. *J. Inorg. Biochem.* **2005**, *99*, 690.
(42) Grapperhaus, C. A.; Mullins, C. S.; Kozlowski, P. M.; Mashuta, M. S. *Inorg. Chem.* **2004**, *43*, 2859.
(43) Seebacher, J.; Ji, M.; Vahrenkamp, H. *Eur. J. Inorg. Chem.* **2004**, 409.
(44) Potenza, M. N.; Stibrany, R. T.; Potenza, J. A.; Schugar, H. J. *Acta Crystallogr.* **1992**, *48*, 454.
(45) Lindoy, L. F.; Lip, H. C.; Rea, J. H.; Smith, R. J.; Henrick, K.; McPartlin, M.; Tasker, P. A. *Inorg. Chem.* **1980**, *19*, 3360.
(46) Shadle, S. E.; Pennerhahn, J. E.; Schugar, H. J.; Hedman, B.; Hodgson, K. O.; Solomon, E. I. *J. Am. Chem. Soc.* **1993**, *115*, 767.
(47) Shadle, S. E.; Hedman, B.; Hodgson, K. O.; Solomon, E. I. *J. Am. Chem. Soc.* **1995**, *117*, 2259.
(48) Solomon, E. I.; Hedman, B.; Hodgson, K. O.; Dey, A.; Szilagyi, R. K. *Coord. Chem. Rev.* **2005**, *249*, 97.
(49) Solomon, E. I.; Penfield, K. W.; Gewirth, A. A.; Lowery, M. D.; Shadle, S. E.; Guckert, J. A.; LaCroix, L. B. *Inorg. Chim. Acta* **1996**, *243*, 67.

(50) Dey, A.; Green, K. N.; Jenkins, R. M.; Jeffrey, S. P.; Darensbourg, M.; Hodgson, K. O.; Hedman, B.; Solomon, E. I. *Inorg. Chem.* **2007**, *46*, 9655.
(51) DeBeer George, S.; Neese, F. *Inorg. Chem.* **2010**, *49*, 1849.
(52) DeBeer George, S.; Petrenko, T.; Neese, F. *Inorg. Chim. Acta* **2008**, *361*, 965.
(53) In the case of **2** and **2Me**, the lowest unoccupied molecular orbital with sulfur and nickel character is actually the LUMO+1.
(54) Kopf, M. A.; Varech, D.; Tuchagues, J. P.; Mansuy, D.; Artaud, I. *J. Chem. Soc., Dalton Trans.* **1998**, 991.
(55) *ABSPACK*; Oxford Diffraction Ltd: Abingdon, Oxfordshire, England, 2010.
(56) Sheldrick, G. M. *SHELXTL*; Madison, WI, 1998.
(57) Neese, F. *ORCA*; Universität Bonn: Bonn, Germany, 2007.
(58) Becke, A. D. *Phys. Rev. A* **1988**, *38*, 3098.
(59) Perdew, J. P. *Phys. Rev. B* **1986**, *33*, 8822.
(60) van Wüllen, C. *J. Chem. Phys.* **1998**, *109*, 392.
(61) van Lenthe, E.; Snijders, J. G.; Baerends, E. J. *J. Chem. Phys.* **1996**, *105*, 6505.
(62) Pantazis, D. A.; Chen, X. Y.; Landis, C. R.; Neese, F. *J. Chem. Theory Comput.* **2008**, 908.
(63) Weigend, F. *Phys. Chem. Chem. Phys.* **2006**, *8*, 1057.